Journal of Ultrafine Grained and Nanostructured Materials
https://jufgnsm.ut.ac.ir
Vol. 56, No.2, December 2023, pp. 213-223
Print ISSN: 2423-6845 Online ISSN: 2423-6837
DOI: 10.22059/jufgnsm.2023.02.10

Effects of Cu addition and heat treatment on the microstructure and hardness of pure Ti prepared by Selective laser melting (SLM)

Mohammad Talebi[1], Ahmad Razaghian[1,*], Abdollah Saboori[2], Behzad Niroumand[3]

[1]Department of Materials Engineering, Imam Khomeini International University (IKIU), Qazvin, 3414896818, Iran;
[2]Department of Management and Production Engineering, Politecnico di Torino, Torino, 10129, Italy;
[3]Department of Materials Engineering, Isfahan University of Technology (IUT), Isfahan, 8415683111, Iran.

Recieved: 1 December 2023; Accepted: 14 December 2023

**Corresponding author email: razaghian@eng.ikiu.ac.ir*

ABSTRACT

Formation of strong texture, columnar grains, and chemical inhomogeneity are some of the serious challenges associated with SLM of metallic alloys. This paper deals with in-situ SLM manufacturing of Ti-5Cu (wt.%) samples from pure Ti and Cu powders at a constant volumetric energy density (VED) of 50.26 J/mm^3. The heat treatment of samples was carried out by heating at 1050 °C (above the β-transus temperature) for 3hr followed by furnace cooling. Then the effects of Cu addition to pure Ti and heat treatment on β-columnar to equiaxed transition (CET) morphology and size of the α phase as well as microhardness of pure Ti and Ti-5Cu samples were investigated. The results showed that the β columnar grains with an average equivalent diameter (d_{eq}) of 80 µm in SLMed pure Ti were effectively converted to equiaxed grains with an average d_{eq} of ~15 µm in the SLMed Ti-5Cu samples. The Cu addition increased the average microhardness from ~290 HV for pure Ti to ~415 HV for Ti-5Cu samples. This was attributed to the formation of equiaxed grains, increased lattice micro-strain resulting from Cu addition and decreased size of the lath-like α phase. The applied heat treatment led to the formation of equiaxed β grains with an average diameter of ~125 µm, dissolution of unmelted titanium particles and the non-dissolution zones of Cu and Ti, and a rather homogeneous structure in Ti-5Cu samples. It also resulted in the decomposition of α′ martensitic structure and the formation of different morphologies of Ti_2Cu precipitates. Reduction of the average microhardness of the Ti-5Cu samples to ~312 HV after heat treatment was also related to the increase in d_{eq} of the equiaxed β grains, in addition to the increase in the size of the α laths phase and decrease in micro-strain.

Keywords: Additive manufacturing, Selective laser melting (SLM), Ti-5Cu alloy, In-situ alloying, columnar to equiaxed transition.

1. Introduction

Additive manufacturing (AM) as an innovative manufacturing method can make parts layer by layer and has many advantages over conventional manufacturing methods such as casting. This is a promising approach to create parts near net shape. This process allows the production of complex geometric objects with waste minimization and minimal time [1]. A faster growth rate (R) of the solidification front due to an increased cooling rate as well as a higher thermal gradient (G) are characteristics of the SLM method compared to other powder bed fusion (PBF) processes [2-4]. The epitaxial growth of columnar grains from the melt pool boundary is a consequence of this effect, which is usually a serious problem in relation to the microstructures resulting from the SLM process. For example, it has been reported that the growth of columnar grains in parts made by additive manufacturing (AM) methods will create

anisotropic mechanical properties [5].

Composition design is a key solution to control the final microstructure of AM-fabricated parts. The importance of chemical composition is related to the influence of alloy elements on the occurrence of columnar to equiaxed transition (CET) phenomenon. This is related to the ability of the solute elements to develop constitutional supercooling (ΔT_{CS}) in front of columnar grains. The effect is characterized as a growth restriction factor (Q), i.e. Eq. 1, where m is the liquidus slope of the phase diagram, C_0 is the solute content of the alloy melt and k_0 is the equilibrium solute partition coefficient [2,6-8].

$$Q = mC_0 (1-k_0) \quad (1)$$

Titanium-based alloys have been considered mainly for the production of orthopedic and dental implants by SLM process due to such features as good biocompatibility, acceptable corrosion properties, and the ability to absorb laser beam [9-12]. On the other hand, the conducted investigations are mainly focused on preventing the formation of columnar grains, and thus anisotropic mechanical properties, in these alloys by adding elements such as Cu [13], Mo [14], B [15], Si [16] and W [17]. Meanwhile, Cu as an alloying element with a high Q factor and unique antibacterial properties has a special ability to create the CET phenomenon and induces increased biological and antibacterial properties in Ti alloys made by AM methods.

In recent years, in-situ alloying by L-PBF technology has eliminated the use of pre-alloyed powders and enabled AM of new alloys with a wide composition range and low cost [9, 18-19]. Mosallanejad et al. [20] reported that the reason for the formation of equiaxed prior β-grains in Ti-1Cu-0.1B alloy produced by L-PBF in-situ alloying is the effect of Cu and B elements on the development of a ΔT_{CS} region and subsequent nucleation of equiaxed prior β- grains on Ti-B precipitates. In another work, with a combination of the inherent capabilities of the electron beam melting (EBM) process, i.e. lower G compared to other AM methods, and the addition of Cu element, Mosallanejad et al. [3] succeeded in creating a fine grained fully equiaxed Ti6Al4V–7Cu alloy sample. Increased microhardness of Ti6Al4V alloy by 7 wt%Cu addition has also been noted as a result of the formation of prior β- grains, solid solution strengthening mechanism, and Ti_2Cu intermetallic precipitation.

Heat treatment has been used as an effective post-processing method after AM processes for various purposes, such as releasing the residual stress, modifying non-equilibrium microstructures to optimize mechanical properties, and homogeneity of chemical composition and uniform distribution of the alloying elements [21-23]. However, in the case of Ti-Cu based alloys, heat treatment has been mostly employed to improve corrosion resistance and bactericidal properties. In a study, stress relieving and annealing treatments of L-PBF Ti_6Al_4V (ELI)-3Cu improved the bactericidal behavior due to the creation of homogenously distributed β phase and Ti_2Cu intermetallic precipitates and as a result of faster release of Cu ions from the β phase [23]. Qin et al. [24] presented a close relationship between the microstructure, distribution pattern of Ti_2Cu phases, heat treatment, and corrosion behavior of SLM-produced Ti-5Cu alloy. The quality of the passive TiO_2 film covering the Ti_2Cu phase depends on how Ti_2Cu is distributed. As a result, for the Ti-5Cu sample heat-treated at 900 °C and then furnace-cooled, larger and more widely spaced Ti_2Cu phases were formed. In this condition, a thicker passive TiO_2 film is formed and, therefore, the corrosion resistance is improved.

Manufacturing parts by the SLM process, however, significantly suppresses the extent of ΔT_{CS} region due to the small size of the laser-melted region, together with the high G, and it poses a challenge to achieve a fine grain size in Ti alloys produced by SLM process. Therefore, adding large Q elements seems necessary to face this challenge. The purpose of this work is to investigate the effect of 5wt.%Cu addition and heat treatment on the transformation of the columnar β grains into equiaxed grains and on the microstructure and microhardness of SLMed pure Ti samples.

2. Materials and methods

In this research, spherical powder of commercially pure Ti powder Grade 1 (≤ 50 μm, LPW, UK), and commercially pure spherical Cu powder (≤ 20 μm, Sandvik Osprey Ltd.) were mixed in a jar mill for 16 hr to prepare homogenous mixtures of Ti-5Cu powders. A Concept Laser Mlab Cusing-R device equipped with a 100 W fiber laser was used to print pure Ti and Ti-5Cu alloy samples. The samples were made in the form of 1×1×1 cm^3 cubes at a constant VED of 50.26 J/mm^3 according to Table 1. The effective spot size of the laser beam and the thickness of the distributed layer were 50 and 25

μm, respectively. The scanning strategy for printing the samples was in the form of a strip with 67° rotations and the oxygen content in the building chamber was kept below 0.1%.

The samples were separated from the titanium substrate by wire electrical discharge machine (WEDM) and were then cut along in build direction with a micro cutter for microstructural analysis on Y-Z surfaces. Some SLMed Ti-5Cu samples were also heat treated for 3 hours at 1050 °C (β solid phase region) in a vacuum furnace at 10^{7-} bar and furnace cooled to room temperature.

Standard metallographic techniques and Kroll's reagent (1wt.%HF, 4wt.%HNO_3 and 95wt.%H_2O) were used to reveal the microstructures. X-ray Diffraction Analyses (XRD, Asenware -AW-XDM300, Cu-Kα radiation), optical microscopy, scanning electron microscopy (SEM: Philips XL30) and field emission electron microscopy (FESEM: Quanta Feg -450) equipped with energy dispersive spectroscopy (EDS) device were carried out on the Y-Z cross sections.

Image J software was used to measure grain size and its distribution. The average size of the equiaxed columnar and grains in the samples was expressed by equivalent diameter (deq, Eq. 2), where A (μm²) is the area of the equiaxed grains.

$$deq = \sqrt{((4*A)/\pi)} \quad (2)$$

Pandat software was employed to plot non-equilibrium diagrams of Scheil, freezing range and calculate the growth restriction factor according to the method proposed by Schmidt-Fetzer and Kezlov [25]. Vickers micro-hardness test was performed using a universal KB250 device and according to the ASTM E384 standard at 1 mm spacings with a static load of 0.5 kg.

3. Results and discussion

Optical micrographs of pure Ti sample manufactured at VED of 50.26 J/mm³ are shown in Fig 1(a). Large epitaxially grown β-columnar grains with a length of several hundred μm are evident in this image. The steep G and the lack of high-Q alloying elements are the main reasons for the formation of undesirable columnar structures in the microstructure of pure Ti parts [26]. Also, the formation of acicular-like α› phase and lath-like α phase can be seen in the form of colonies not only in the prior β grain boundaries but also inside the β-columnar grains and in some areas of the microstructure in Fig. 1 (a). The formation of the acicular-like α› phase is a result of the rapid cooling of the β phase from β transus temperature, which can be clearly seen in Fig. 1 (b) at a higher magnification. The average width of the acicular-like α› phase and lath-like α phase was measured by the image analysis method to be ~ 0.66∓0.22 and 4.23∓0.92 μm, respectively. In addition, the α phase is formed as irregular or close to equiaxed and elongated α grains in some points of the microstructure and

Table 1- The SLM process parameter used to build different samples

Sample	Ti	Ti-5Cu
VED (*J/mm³*)	50.26	50.26
Scanning speed (*mm/s*)	700	700
Hatch Spacing (*mm*)	0.108	0.108
Laser Power (*W*)	95	95

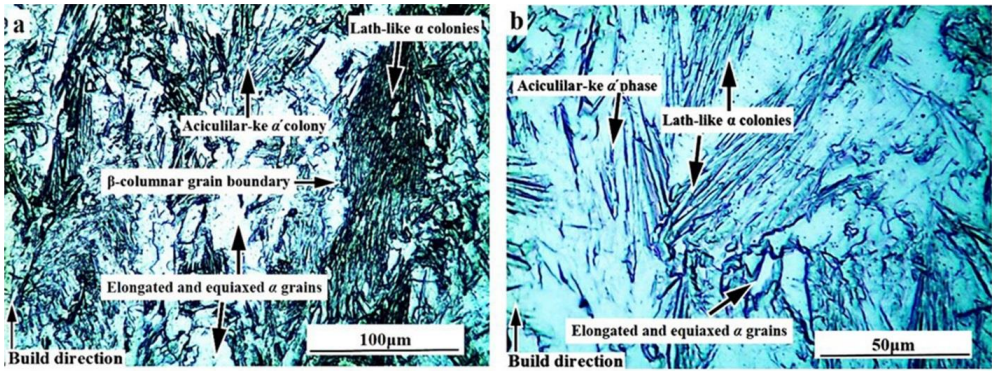

Fig. 1- Micrographs of pure titanium sample produced at VED of 50.26 J/mm³.

also as α-grain boundaries (α_{GB}) along some of the prior β grain boundaries (Fig. 1 (a)). Due to the manufacturing of pure Ti sample at VED of 50.26 J/mm^3, it seems that the Ti powders have not been completely melted and distributed in some areas, and therefore, the lower cooling rate of these powders compared to other areas prevented the formation of acicular-like α› and lath-like α phases. This has led to the formation of different morphologies of the α phase in the microstructure of pure Ti, such as elongated and equiaxed grains. Wysocki et al. [27] also investigated the microstructure of pure Ti made by the SLM process and reported the formation of irregular or close to equiaxed α grains on the prior β grain boundaries. Varying laser scanning speed (V) produces different morphologies of α and α› phases in the microstructure of pure Ti [28, 29]. For example, increasing V from 0.02 to 0.2 m/s under a constant laser power (P) of 100 W resulted in the transformation of the coarse lath-like α phase into the acicular-like α› phase [29]. This was attributed to the different cooling rates in the SLM process which is directly affected by G and V [28].

Fig. 2 shows the optical microstructure of the Ti-5Cu sample fabricated at VED of 50.26 J/mm^3, which clearly shows that columnar β grains in the Ti microstructure (Fig. 1(a)) have turned into equiaxed β grains in some regions of the microstructure. Also, as shown in Fig. 2(c), in other parts of the microstructure, the average width of the columnar grains has decreased to 3 μm. In fact, a larger number of narrower columnar grains have been formed than those in the microstructure of pure Ti. Because pure Ti sample and Ti-5Cu alloy samples were produced in the same VED, formation, size reduction, and increase in the number of equiaxed β grains by adding Cu in the microstructure of Ti-5Cu samples can be due to the high potency of Cu solute atoms to create large ΔT_{CS} zone in front of the solidification front. The rate at which a solute element can create ΔT_{CS} is predicted by Q [8]. In this research, the value of Q for Ti-5Cu alloy was calculated by the method proposed by Schmidt-Fetzer and Kezlov [25] in scheil non-equilibrium conditions and using PANDAT software data. In this way, Q for Ti-5Cu alloy was obtained as 35 K.

According to the interdependence theory [30], the key factors controlling the grain size include the critical undercooling for nucleation (ΔT_n), ΔT_{CS}, and the average spacing between the potent nucleation particles (X_{sd}). So a small ΔT_n, large ΔT_{CS}, and small X_{sd} help the grain refinement, e.g. a larger Q causes more nucleation.

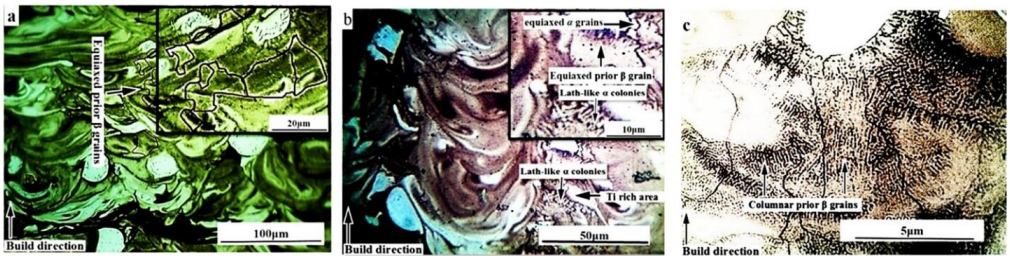

Fig. 2- Optical microstructure of Ti-5Cu samples at VED of 50.26 J/mm^3.

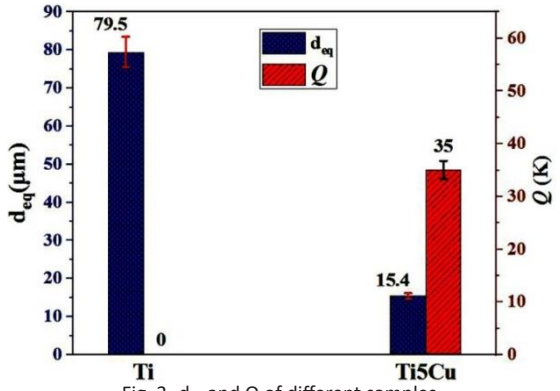

Fig. 3- d_{eq} and Q of different samples.

The column chart of Fig. 3 shows the changes in the average prior β grain equivalent diameter (d_{eq}) and Q of the two samples. As can be seen, d_{eq} of β grains decreases from 79.5 for the pure Ti samples to 15.4 μm for the as-built Ti-5Cu samples simultaneously with the increase of Q from 0 to 35 K.

Comparing the colonies and also the different morphologies of the α phase in the microstructure of pure Ti (Fig. 1) with those of the α phase in the microstructure of the as-built Ti-5Cu sample (Fig. 2(b)), a decrease in the number and size of the α colonies in the microstructure of the as-built Ti-5Cu sample is clear. However, these are limited only to small isolated colonies scattered at the border of unmelted Ti particles, Ti rich areas, and inside small equiaxed prior β grains.

As shown in the SEM and optical images of the as-built Ti-5Cu microstructure (Fig. 4(a) and 2(b)), the formation of the lath-like α colonies occurs on the boundaries of Ti rich areas. On the other hand, the size of lath-like α phase and equiaxed α grains in the microstructure of the as-built Ti-5Cu sample is greatly reduced compared to the pure Ti sample. The average values of length, width, and aspect ratio of intragranular and intergranular lath-like α phase of pure Ti and the as-built Ti-5Cu samples were calculated by recording more than 100 lath-like α phase and by image analysis technique (Table 2). The average length and width of α laths decreased from 15.94 and 2.83 μm in the in the microstructure of pure Ti sample to 5.8 and 1.5 μm in the microstructure of as-built Ti-5Cu samples, respectively. On the other hand, with the average reduction of aspect ratio from ~ 6.4 for the pure Ti sample to ~ 3.2 for the as-built Ti-5Cu sample, it is clear that the lath-like α phase tends to be more equiaxed.

Previous investigations mentioned several main reasons for the reduction in the size of large grain boundary and intragranular α colonies in the microstructure of Ti_6Al_4V alloy with the addition of B element [31- 34]. Reduction of the prior β grain size with increasing B content restricts the growth space of the intragranular α phase. On the other hand, the disintegration of the continuous α_{GB} by adding element B increases the number of α phase nucleation on the broken α_{GB}. Furthermore, the high potent TiB nucleant is mentioned as another reason for reducing the size of α colonies. Also, these studies consider the reasons for the significant decrease in the size of the α laths similar to the decrease in the size of α colonies, to be related to the reduction of the previous β grains and the high potent TiB phase heterogeneous nucleation

Table 2- Measured values for the length, width and aspect ratio of the lath-like α phase in pure Ti and Ti-5Cu microstructures

Sample	Length (*μm*)	Width (*μm*)	Aspect ratio
Ti	15.94	2.83	6.44
Ti-5Cu	5.8	1.5	3.25

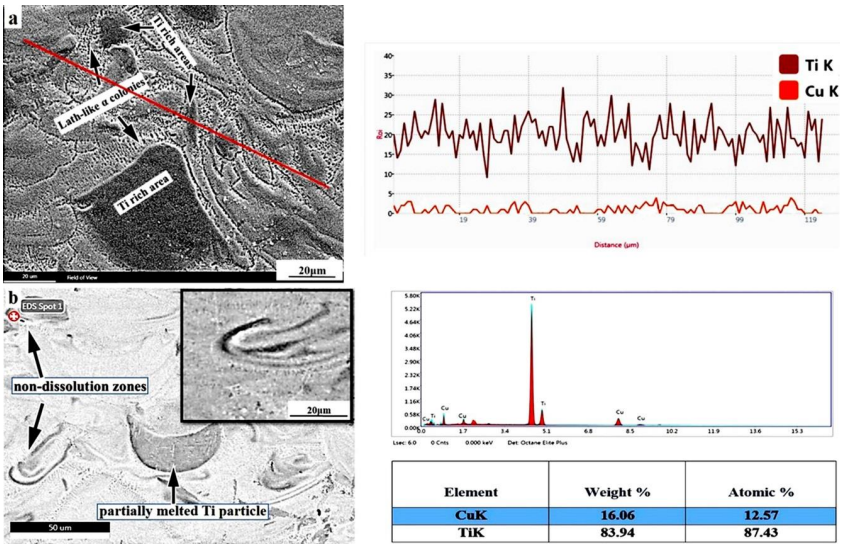

Element	Weight %	Atomic %
CuK	16.06	12.57
TiK	83.94	87.43

Fig. 4- a) SEM image with EDS line analysis and b) FESEM image with EDS point analysis from the microstructure of Ti-5Cu sample.

site [33, 34]. Therefore, according to the previous findings, a decrease in the size of the α colonies and the α laths can be attributed to the decreased size of the previous β grains due to the addition of Cu element.

The chemical homogeneity of the as-built Ti-5Cu sample was investigated using field emission scanning electron microscope (FESEM), SEM, and energy dispersive spectroscopy (EDS) techniques. The distribution of Ti and Cu elements in different points of the microstructure for the as-built Ti-5Cu sample was investigated by SEM image and EDS line analysis, and the results are reported in Fig. 4(a). The extreme fluctuations of these elements in the as-built Ti-5Cu microstructure have occurred due to the lack of complete mixing of different elements. Fig. 4(b) shows areas of the microstructure with non-uniform mixing of Ti and Cu elements as well as Ti -rich pools that have not been completely melted by the laser beam. Although in the non-dissolution zone, the local segregation of Cu has occurred as a vein shape next to the Ti-rich zone. Also, the results of the EDS point analysis of this area (Fig. 4(b)) showed the Cu content at around 16 wt%, which reveals the lack of complete dissolution of Ti and Cu elements in this area. Complete melting of powders is a necessary condition for in situ alloying. Even if the powders are completely melted, the difference in viscosity and density between the components in the liquid state during in situ alloying may lead to chemical inhomogeneity [18, 35].

Fig. 5 shows the microstructure of the Ti-5Cu sample made under VED of 50.26 J/mm^3 and heat treated at 1050 °C. The microstructure of the heat-treated Ti–5Cu sample has undergone many microstructural changes compared to the microstructure of the as-built sample shown in Fig. 2. As shown in Fig. 5 (a), heat treatment above the β-transus temperature (1050 °C) results in dissolving all columnar β grains in the as-built Ti-5Cu microstructure (Fig. 2 (c)) and forming a fully equiaxed structure of prior-β grains. On the other hand, the extensive β grains growth compared to those in the as-built microstructure occurs, and the large prior-β grains are formed with deq equal to 125.5 μm. Previous observations reported that the dissolution of columnar grains and formation of equiaxed grains after heat treatment above the β-transus temperature is related to the growth rate of α phase [36, 37]. Considering that both α and β phases tend to become coarser at higher temperatures, they hinder each other's growth. In addition, the presence of the αGB phase at temperatures lower than the β-transus temperature prevents the growth of columnar grains and columnar to equiaxed transition [36, 37]. Therefore, heat treatment within the range of β single phase causes the growth of β grains without any restrictions. Su et al. [21] reported that heat treatment of Ti-6Al-4V- SLMed samples at a temperature above the β-transus temperature (1100 °C) resulted in the formation of equiaxed β grains instead of columnar β grains, while heat treatment at temperatures below the β-transus temperature (850 °C) preserved columnar β grains.

As shown in Fig. 5, a thin layer of α_{GB} is continuously formed along the entire prior β grain boundaries. A slow cooling rate, i.e., ~ 1.5 °C/s above the β-transus temperature, causes the nucleation of the

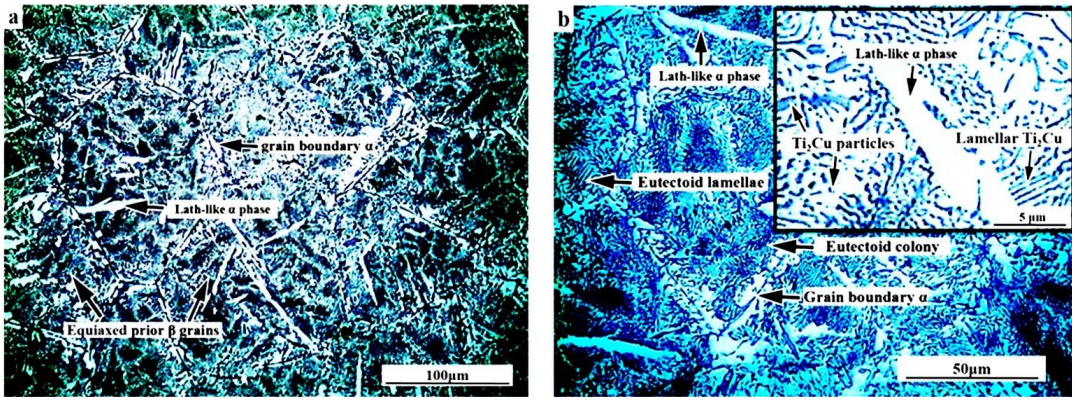

Fig. 5- a) Optical micrographs of Ti-5Cu samples manufacturing at VED of 50.26 J/mm^3 and the heat-treated at 1050 °C and b) higher magnification of a) showing Ti_2Cu intermetallic phases.

α phase preferentially at the β grain boundaries and because the β grain boundaries act as an effective nucleation site, a continuous layer of α_{GB} is formed [38]. Heating up to β zone (1050 °C) led to the decomposition of α´ martensitic phase, destroyed unmelted/partially melted Ti particles and the areas with incomplete dissolution of Cu and Ti, due to the increase in diffusion rates of solute atoms and reduction in the difference in viscosity and density of liquid Cu and liquid Ti. In these conditions, a structure with a relatively homogeneous distribution of all elements is formed. The slow cooling process (furnace cooling) allows the eutectoid transformation to take place and thus a lamellar eutectoid arrangement of α-Ti (light color) and Ti_2Cu (dark color) from the β phase decomposition can be clearly observed in the microstructure of the heat-treated Ti–5Cu sample (Fig. 5(b)).

It can be noticed in the optical micrograph (Fig. 5(b)) and the SEM image (Fig. 6) that Cu-rich intermetallic compound is formed with different morphologies including blocky (3-5 μm), submicron-sized (200-500 nm), short lath and lamellar or sheaf Ti_2Cu precipitates. The EDS line profile in Fig. 6(b) shows the element gradient on successive Cu-rich intermetallic layers and adjacent α phase, and confirms the precipitation of the Ti_2Cu intermetallic phase. On the other hand, the α_{GB} phase and Ti_2Cu precipitates can be distinguished by evaluating the Cu and Ti EDS maps shown in Fig. 6(c). Zhao et al. [39] reported a conversion from the lamellar α+Ti_2Cu structure combined with the blocky peritectic Ti_2Cu precipitates to short laths and blocky Ti_2Cu as a result of increasing the cooling rate from furnace cooling to water cooling in Ti-13Cu-Al alloy. It is considered that the different morphologies of the subsequent eutectoid phase originated from different nucleation sites of the peritectic Ti_2Cu phase which is affected by the cooling rate. The sheaves morphology of eutectoid structure (α+Ti_2Cu) is created in the high cooling rate condition and when the eutectoid Ti_2Cu nucleates on the blocky Ti_2Cu phase which is formed by the peritectic reaction from the β/L interface [39].

It was shown by Mosallanejad et al. [3] that the successive stages of re-melting and refreezing of previously solidified layers during the EBM process induced heating and cooling cycles of annealing and aging. Subsequently, Ti_2Cu precipitates were formed with different morphologies including blocky, irregular, and submicron-sized in the microstructure of Ti6Al4V-7Cu Alloy. Ti_2Cu precipitates with different morphologies and sizes were also reported by previous studies during annealing and solution heat treatment [23, 39, 40]. Annealing of Ti6Al4V (ELI)-3at.%Cu alloy produced by in-situ laser powder bed fusion (L-PBF) method for 2 h at 950 °C and slow cooling in a furnace for 4 hr changed the size and morphology of Ti_2Cu intermetallic precipitates and turned them into more elongated-shape precipitates (from 200 nm to 1.5 μm) [23]. Previous findings in terms of changing the morphology and size of Ti_2Cu precipitates by different cooling rates are in line with the findings of the current report. According to the current results, the presence of unmelted/partially melted Ti particles in the microstructure of the as-built Ti-5Cu sample (Fig. 2) causes different cooling rates during the heat treatment cycle at different points of the microstructure, and therefore, varied morphologies of Ti_2Cu precipitates appear in the microstructure of the heat-treated Ti–5Cu sample. Also, due to the dissolution of unmelted/partially melted Ti particles at 1050°C, laths-like α phase

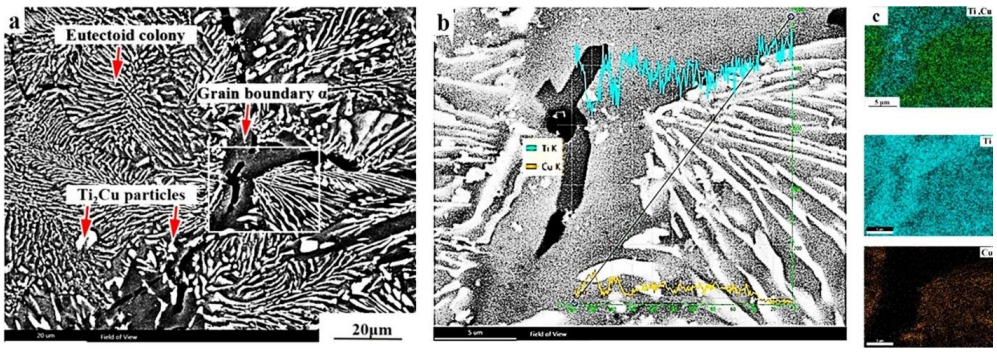

Fig. 6- a) a) SEM image of Ti-5Cu samples manufacturing at VED of 50.26 J/mm³ and the heat-treated at 1050°c, b) higher magnification of a) with the EDS line scan and c) EDS map of Cu and Ti in (b).

with an average size of 24.3 μm have been formed in the microstructure of the heat- treated Ti-5Cu sample (Fig. 5) compared to those in the microstructure of the as-built sample (Fig. 2). Fig. 7 (a) shows the X-ray diffraction (XRD) patterns of pure Ti, the as-built Ti-5Cu, and the heat-treated Ti-5Cu samples. Most of the peaks are assigned to the α/α' phase. The β phase (110) peaks are created after Cu addition, but due to the overlap of the α/α› phase (002) peaks, they cannot be recognized. After the heat treatment, peaks of the Ti_2Cu phase were identified in the XRD pattern in Fig. 7 (a). A transition to larger diffraction angles related to all the peaks of the α/α› phase has occurred with the addition of Cu element (Fig. 7 (b)). This transition can be explained by considering the fact that the increase in atomic radius difference between Ti and Cu and elements can create different micro-strains in the Ti crystal lattice [3].

Given the fact that the atomic radius of Cu (0.128 nm) is about 12% smaller than that of Ti (0.147 nm), Cu would dissolve substitutionally in the α lattice leading to a reduction of the inter-planar spacing in Ti crystal structure [3]. By examining Fig. 7 (b), it can be seen that the transition to larger diffraction angles for the α phase of the heat-treated Ti-5Cu sample is much less than that of the as-built Ti-5Cu sample, resulting in reduced lattice microstrain of the heat-treated Ti-5Cu sample. This can be due to the equilibrium placement of Cu atoms in the Ti HCP crystal lattice. This difference in lattice microstrain by adding Cu element to pure Ti, and performing the heat treatment respectively, can be found by comparing the slope of the Williamson-Hall plots related to pure Ti, the as-built Ti-5Cu and the heat-treated Ti-5Cu samples. As can be seen by comparing Figure 8 (a), (b), and (c), the slope of the Williamson-Hall diagrams increased after adding Cu to pure Ti and decreased again after heat treatment. The lattice microstrain changes for the pure Ti, the as-built Ti-5Cu, and the heat-treated Ti-5Cu samples were calculated from the slope of the Williamson-Hall plots and are shown in Figure 9 (a).

The average microhardness of the pure Ti, the as-built Ti-5Cu, and the heat-treated Ti-5Cu samples are shown in Fig. 10. The average Vickers hardness for the as-built Ti-5Cu samples is 415±0.61 HV with the minimum and maximum measured values of 385 and 445 HV, respectively. On the other hand, these values for the Ti sample are 290 ± 0.54, 263, and 328 HV, respectively. The increase in

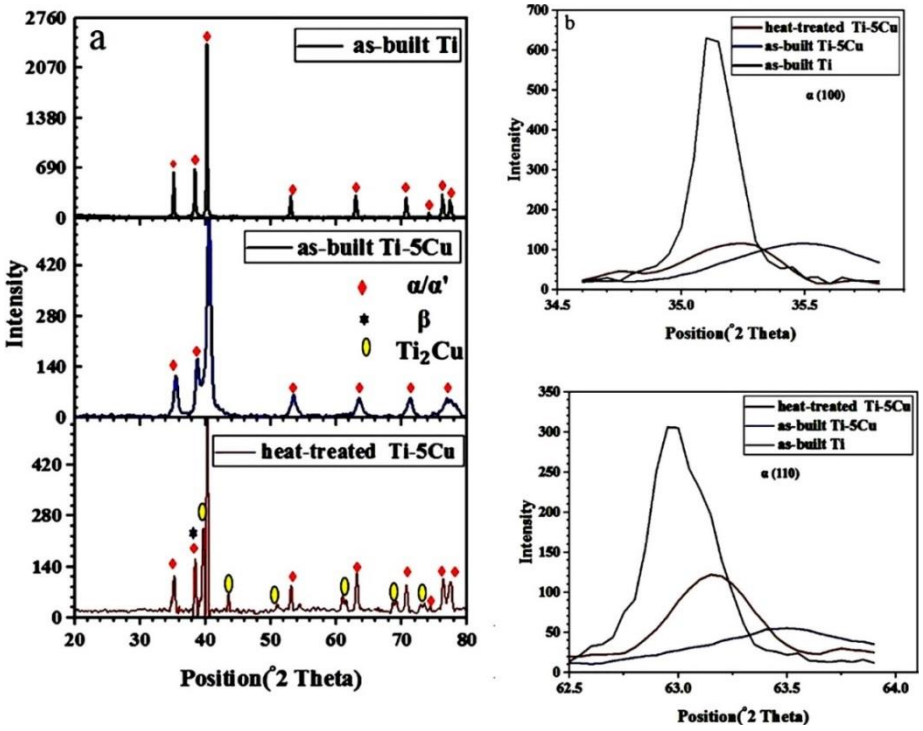

Fig. 7- (a) XRD patterns of pure Ti, as-built Ti-5Cu and heat-treated Ti-5Cu samples and (b) enlarged profiles of α (100) and α (110) peaks.

hardness of the as-built Ti-5Cu sample compared to pure Ti can be evaluated from several aspects. Firstly, the results are consistent with the decrease in the grain size of the Ti-5Cu sample. Furthermore, the increase in the hardness resulting from the Cu addition is partly due to the solid solution strengthening of the β-phase with a larger amount of dissolved Cu and the formation of equiaxed grains [3, 20]. Also, induced lattice microstrain due to the Cu addition limits the slip planes in the HCP structure.

The employed heat treatment has decreased the average microhardness to 312±0.45 HV. This can be attributed to the simultaneous increase in d_{eq} of the equiaxed prior β-grains and the lath-like α phase by heat treatment. Galaraga [22] presented an inverse relationship between lath-like α width and microhardness assuming that microstructural features act as barriers to dislocation slip and cause the dislocation pileup. Therefore, one notable reason for the decrease in the microhardness of the heat-treated Ti-5Cu sample is the growth of the

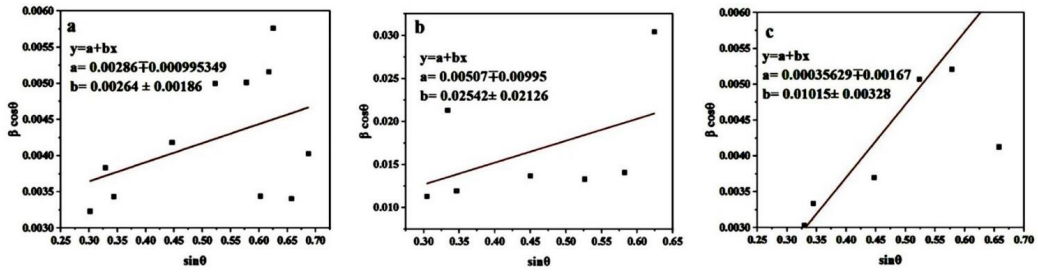

Fig. 8- Williamson-Hall plots for a) CP Ti, b) as-built Ti-5Cu and c) heat-treated Ti-5Cu samples.

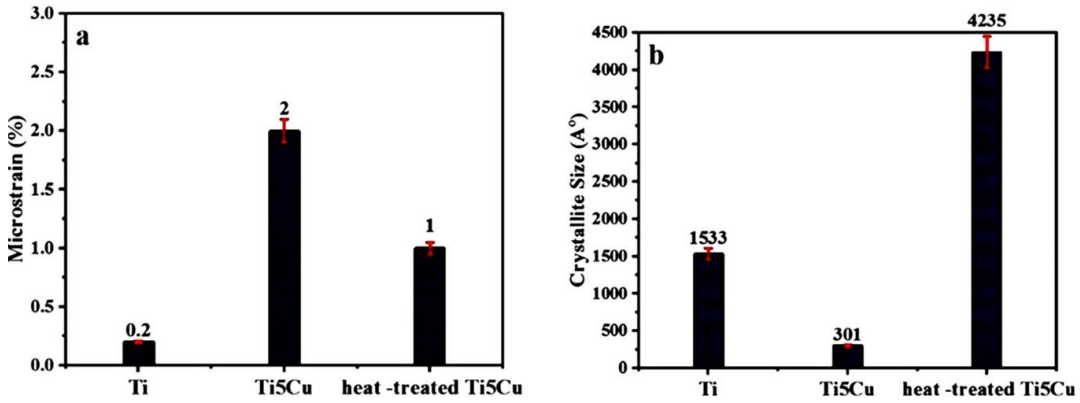

Fig. 9- Variation diagrams of (a) α lattice micro-strain and (b) α crystallite size for the pure Ti, the as-built Ti-5Cu and the heat-treated Ti-5Cu samples.

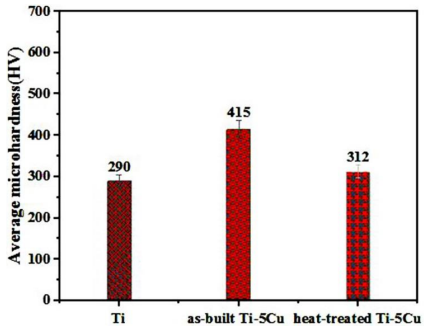

Fig. 10- Changes in Vickers microhardness for Ti, Ti-5Cu and heat-treated Ti-5Cu samples.

lath-like α phase. Also, the reduction of lattice microstrain due to heat treatment leads to an increase in the slip system in the titanium crystal lattice, and as a result, microhardness decreases. The research conducted in relation to the Si addition to Ti shows that the restriction of slip planes in the hcp structure due to lattice microstrain increases the hardness of Ti-Si alloy [43].

Conclusions

Ti and in-situ synthesized Ti-5Cu samples were printed via the SLM process. Also, the as-built Ti-5Cu samples were subjected to heat treatment at 1050 °C for 3 h and furnace cooling to room temperature, and the effects of Cu addition and heat treatment on the microstructural and microhardness characteristics of the samples were investigated. The main results follow;

1- Addition of 5wt%Cu to pure Ti led to the transition of columnar β grains in the pure Ti sample to equiaxed grains with an average equivalent diameter of 15.4 μm in the Ti-5Cu samples.

2- The average length, width, and aspect ratio of the lath-like α phase decreased from 15.94, 2.83 μm and 6.44 in the microstructure of pure Ti to 5.8, 1.5 μm and 3.25 in the microstructure of the as-built Ti-5Cu sample.

3- The number and size of the α colonies in the microstructure decreased with the addition of 5wt%Cu to pure Ti. The Cu addition increased the lattice microstrains in the microstructure of the as-built Ti-5Cu sample.

4- The average microhardness of the pure Ti sample was measured as 290 ± 0.54 HV, which increased to 415±0.61 HV for the Ti-5Cu sample due to decreased grain size, reduced width of the lath-like α phase and the columnar to equiaxed β grains transition.

5- The employed heat treatment led to the dissolution of unmelted Ti particles and the complete solubility of the non-dissolution zone of Cu and Ti and improved homogeneity of the microstructure.

6- A collection of Ti_2Cu precipitates with different morphologies including blocky, submicron-sized, short lath, and lamellar were precipitated after heat treatment in the microstructure of heat-treated Ti-5Cu samples.

7- The employed heat treatment led to an increase in the average equivalent diameter of the equiaxed β grains, the average size of the lath-like α phase, and decreases microhardness resulting in a decrease in the average microhardness of the Ti-5Cu samples to 312±0.45 HV.

References

1. Zhang D, Sun S, Qiu D, Gibson MA, Dargusch MS, Brandt M, et al. Metal Alloys for Fusion-Based Additive Manufacturing. Advanced Engineering Materials. 2018;20(5).
2. Collins PC, Brice DA, Samimi P, Ghamarian I, Fraser HL. Microstructural Control of Additively Manufactured Metallic Materials. Annual Review of Materials Research. 2016;46(1):63-91.
3. Mosallanejad MH, Niroumand B, Ghibaudo C, Biamino S, Salmi A, Fino P, Saboori A. In-situ alloying of a fine grained fully equiaxed Ti-based alloy via electron beam powder bed fusion additive manufacturing process. Additive Manufacturing. 2022;56:102878.
4. Leung CLA, Tosi R, Muzangaza E, Nonni S, Withers PJ, Lee PD. Effect of preheating on the thermal, microstructural and mechanical properties of selective electron beam melted Ti-6Al-4V components. Materials & Design. 2019;174:107792.
5. Carroll BE, Palmer TA, Beese AM. Anisotropic tensile behavior of Ti–6Al–4V components fabricated with directed energy deposition additive manufacturing. Acta Materialia. 2015;87:309-20.
6. M. J. Bermingham, D. H, StJohn, b. J. Krynen, S. Tedman-Jones, M. S. Dargusch, Promoting the columnar to equiaxed transition and grain refinement of titanium alloys during additive manufacturing, Acta Mater., 168, 2019, 261–274.
7. Fan Z, Gao F, Zhou L, Lu SZ. A new concept for growth restriction during solidification. Acta Materialia. 2018;152:248-57.
8. Bermingham M, StJohn D, Easton M, Yuan L, Dargusch M. Revealing the Mechanisms of Grain Nucleation and Formation During Additive Manufacturing. JOM. 2020;72(3):1065-73.
9. Vilardell AM, Takezawa A, du Plessis A, Takata N, Krakhmalev P, Kobashi M, et al. Mechanical behavior of in-situ alloyed Ti6Al4V(ELI)-3 at.% Cu lattice structures manufactured by laser powder bed fusion and designed for implant applications. Journal of the Mechanical Behavior of Biomedical Materials. 2021;113:104130.
10. Del Guercio G, Galati M, Saboori A, Fino P, Iuliano L. Microstructure and Mechanical Performance of Ti–6Al–4V Lattice Structures Manufactured via Electron Beam Melting (EBM): A Review. Acta Metallurgica Sinica (English Letters). 2020;33(2):183-203.
11. Abdel-Hady Gepreel M, Niinomi M. Biocompatibility of Ti-alloys for long-term implantation. Journal of the Mechanical Behavior of Biomedical Materials. 2013;20:407-15.
12. Xu X, Lu Y, Li S, Guo S, He M, Luo K, Lin J. Copper-modified Ti6Al4V alloy fabricated by selective laser melting with pro-angiogenic and anti-inflammatory properties for potential guided bone regeneration applications. Materials Science and Engineering: C. 2018;90:198-210.
13. Zhang D, Qiu D, Gibson MA, Zheng Y, Fraser HL, StJohn DH, Easton MA. Additive manufacturing of ultrafine-grained high-strength titanium alloys. Nature. 2019;576(7785):91-5.
14. Zhang F, Mei M, Al-Hamdani K, Tan H, Clare AT. Novel nucleation mechanisms through satelliting in direct metal deposition of Ti-15Mo. Materials Letters. 2018;213:197-200.
15. Mantri SA, Alam T, Choudhuri D, Yannetta CJ, Mikler CV, Collins PC, Banerjee R. The effect of boron on the grain size and texture in additively manufactured β-Ti alloys. Journal of Materials Science. 2017;52(20):12455-66.
16. Mereddy S, Bermingham MJ, StJohn DH, Dargusch MS. Grain refinement of wire arc additively manufactured titanium

by the addition of silicon. Journal of Alloys and Compounds. 2017;695:2097-103.
17. Mendoza MY, Samimi P, Brice DA, Martin BW, Rolchigo MR, LeSar R, Collins PC. Microstructures and Grain Refinement of Additive-Manufactured Ti-xW Alloys. Metallurgical and Materials Transactions A. 2017;48(7):3594-605.
18. Krakhmalev P, Yadroitsev I, Yadroitsava I, de Smidt O. Functionalization of Biomedical Ti6Al4V via In Situ Alloying by Cu during Laser Powder Bed Fusion Manufacturing. Materials (Basel). 2017;10(10):1154.
19. Mosallanejad MH, Niroumand B, Aversa A, Saboori A. In-situ alloying in laser-based additive manufacturing processes: A critical review. Journal of Alloys and Compounds. 2021;872:159567.
20. Mosallanejad MH, Niroumand B, Ghibaudo C, Biamino S, Salmi A, Fino P, Saboori A. In-situ alloying of a fine grained fully equiaxed Ti-based alloy via electron beam powder bed fusion additive manufacturing process. Additive Manufacturing. 2022;56:102878.
21 Su C, Yu H, Wang Z, Yang J, Zeng X. Controlling the tensile and fatigue properties of selective laser melted Ti–6Al–4V alloy by post treatment. Journal of Alloys and Compounds. 2021;857:157552.
22 Galarraga H, Warren RJ, Lados DA, Dehoff RR, Kirka MM, Nandwana P. Effects of heat treatments on microstructure and properties of Ti-6Al-4V ELI alloy fabricated by electron beam melting (EBM). Materials Science and Engineering: A. 2017;685:417-28.
23. Martín Vilardell A, Cantillo Alzamora V, Bauso LV, Madrid C, Krakhmalev P, Albu M, et al. Effect of Heat Treatment on Osteoblast Performance and Bactericidal Behavior of Ti6Al4V(ELI)-3at.%Cu Fabricated by Laser Powder Bed Fusion. J Funct Biomater. 2023;14(2):63.
24. Qin P, Liu Y, Sercombe TB, Li Y, Zhang C, Cao C, et al. Improved Corrosion Resistance on Selective Laser Melting Produced Ti-5Cu Alloy after Heat Treatment. ACS Biomaterials Science & Engineering. 2018;4(7):2633-42.
25. Schmid-Fetzer R, Kozlov A. Thermodynamic aspects of grain growth restriction in multicomponent alloy solidification. Acta Materialia. 2011;59(15):6133-44.
26. Liu S, Shin YC. Additive manufacturing of Ti6Al4V alloy: A review. Materials & Design. 2019;164:107552.
27. Wysocki B, Maj P, Krawczyńska A, Rożniatowski K, Zdunek J, Kurzydłowski KJ, Święszkowski W. Microstructure and mechanical properties investigation of CP titanium processed by selective laser melting (SLM). Journal of Materials Processing Technology. 2017;241:13-23.
28. Li XP, Van Humbeeck J, Kruth JP. Selective laser melting of weak-textured commercially pure titanium with high strength and ductility: A study from laser power perspective. Materials & Design. 2017;116:352-8.
29. Zhang B, Liao H, Coddet C. Microstructure evolution and density behavior of CP Ti parts elaborated by Self-developed vacuum selective laser melting system. Applied Surface Science. 2013;279:310-6.
30. StJohn DH, Qian M, Easton MA, Cao P. The Interdependence Theory: The relationship between grain formation and nucleant selection. Acta Materialia. 2011;59(12):4907-21.
31. Mantri SA, Alam T, Choudhuri D, Yannetta CJ, Mikler CV, Collins PC, Banerjee R. The effect of boron on the grain size and texture in additively manufactured β-Ti alloys. Journal of Materials Science. 2017;52(20):12455-66.
32. Xue A, Wang L, Lin X, Wang J, Chen J, Huang W. Effect of boron on the microstructure and mechanical properties of Ti-6Al-4V produced by laser directed energy deposition after heat treatment. Journal of Laser Applications. 2020;32(1).
33. Xue A, Lin X, Wang L, Wang J, Huang W. Influence of trace boron addition on microstructure, tensile properties and their anisotropy of Ti6Al4V fabricated by laser directed energy deposition. Materials & Design. 2019;181:107943.
34. Zhang K, Tian X, Bermingham M, Rao J, Jia Q, Zhu Y, et al. Effects of boron addition on microstructures and mechanical properties of Ti-6Al-4V manufactured by direct laser deposition. Materials & Design. 2019;184:108191.
35. Yadroitsev I, Krakhmalev P, Yadroitsava I. Titanium Alloys Manufactured by In Situ Alloying During Laser Powder Bed Fusion. JOM. 2017;69(12):2725-30.
36. Vrancken B, Thijs L, Kruth J-P, Van Humbeeck J. Heat treatment of Ti6Al4V produced by Selective Laser Melting: Microstructure and mechanical properties. Journal of Alloys and Compounds. 2012;541:177-85.
37. Raghavan S, Nai MLS, Wang P, Sin WJ, Li T, Wei J. Heat treatment of electron beam melted (EBM) Ti-6Al-4V: microstructure to mechanical property correlations. Rapid Prototyping Journal. 2018;24(4):774-83.
38. Donachie MJ. Titanium: a technical guide. ASM international; 2000.
39. Zhao D, Chen Y, Jiang C, Li Y, Zhao Q, Xu Y, et al. Morphological evolution of Ti2Cu in Ti-13Cu-Al alloy after cooling from semi-solid state. Journal of Alloys and Compounds. 2020;848:156639.
40. Yadav P, Saxena KK. Effect of heat-treatment on microstructure and mechanical properties of Ti alloys: An overview. Materials Today: Proceedings. 2020;26:2546-57.
41. Hemmasian Ettefagh A, Zeng C, Guo S, Raush J. Corrosion behavior of additively manufactured Ti-6Al-4V parts and the effect of post annealing. Additive Manufacturing. 2019;28:252-8.
42. Li L, Chen Y, Lu Y, Qin S, Huang G, Huang T, Lin J. Effect of heat treatment on the corrosion resistance of selective laser melted Ti6Al4V3Cu alloy. Journal of Materials Research and Technology. 2021;12:904-15.
43. Oh JM, Lim JW, Lee BG, Suh CY, Cho SW, Lee SW, Choi GS. Grain Refinement and Hardness Increase of Titanium via Trace Element Addition. MATERIALS TRANSACTIONS. 2010;51(11):2009-12.